Lattice Boltzmann model for the one-dimensional nonlinear Dirac equation

Baochang Shi*
School of Mathematics and Statistics, Huazhong University of Science and Technology, Wuhan 430074, People's Republic of China

Zhaoli Guo†
State Key Laboratory of Coal Combustion, Huazhong University of Science and Technology, Wuhan 430074, People's Republic of China

(Received 24 December 2008; revised manuscript received 9 May 2009; published 5 June 2009)

In this paper, a lattice Boltzmann model for one-dimensional nonlinear Dirac equation is presented by using double complex-valued distribution functions and carefully selected equilibrium distribution functions. The effects of space and time resolutions and relaxation time on the accuracy and stability of the model are numerically investigated in detail. It is found that the model is of second-order accuracy in both space and time, and the order of accuracy is near 3.0 at lower grid resolution, which shows that the lattice Boltzmann method is an effective numerical scheme for the nonlinear Dirac equation.

DOI: 10.1103/PhysRevE.79.066704 PACS number(s): 02.70.−c, 02.60.Cb, 05.45.Yv

I. INTRODUCTION

The lattice Boltzmann method (LBM) is a promising technique for simulating fluid flows and modeling complex physics in fluids [1–3]. Compared with the conventional computational fluid dynamics approaches, the LBM is easy for programming, intrinsically parallel, and it is also easy to include complicated boundary conditions such as those in porous media. Up to now, the most widely used LBM is the so-called lattice Bhatnagar-Gross-Krook (LBGK) model. However, the LBGK model may suffer from numerical instability when it is used to simulate the fluid with small viscosity. A lot of work has been done to improve the stability of the lattice Boltzmann (LB) model, among which the multi-relaxation-time LBM [4–6] and entropic LBM [7–11] have attracted much attention in recent years. It should be noted that the LBM also shows potentials to simulate the nonlinear systems, such as reaction-diffusion equation [12–14], convection-diffusion equation (CDE) [15–20], Burgers equation [21], Korteweg-de Vries equation [22], Poisson equation [23], etc. However, they are commonly limited to isotropic diffusions. Recently, the LB models for advection and anisotropic dispersion equation have been proposed [24–26], among which the model proposed by Ginzburg [26] is generic. Van der Sman and Ernst deeply studied the LBM for CDE and presented several LB schemes on rectangular or irregular lattices (see Refs. [18,19] and references therein).

Most of the existing LB models are used for real nonlinear systems. Since the middle of 1990s, several types of quantum lattice gases and quantum LBM have been proposed based on quantum-computing ideas to model some real and complex mathematical-physical equations, such as the Dirac equation, Schrödinger equation, Gross-Pitaevskii equation, Burgers equation, KdV equation [27–36], etc. We refer the readers to a recent paper [36] for a detailed review. On the other hand, recently, the classical LB model has been used to model complex equations. In Ref. [37] the LBM was applied to a one-dimensional (1D) nonlinear Schrödinger equation (NLSE) following the idea of quantum lattice-gas model [30,31] to treat the reaction term. The simulation results show that the accuracy of the LB schemes was better than or at least comparable to that of the Crank-Nicolson finite difference scheme. In Ref. [38], motivated by the work in Ref. [37], the LBM for n-dimensional (nD) CDE with a source term was directly applied to some nonlinear complex equations, including the NLSE, coupled NLSEs, Klein-Gordon equation, and coupled Klein-Gordon-Schrödinger equations, by adopting a complex-valued distribution function and relaxation time. In Ref. [39], we presented a LB model for a general class of nD CDEs with nonlinear convection and isotropic-diffusion terms by properly selecting equilibrium distribution function. The model can be applied to both real and complex-valued nonlinear evolutionary equations. The studies in Refs. [37–39] show that the LBM may be an effective numerical solver for real and complex-valued nonlinear systems. Therefore, it is worthy to study LBM and enlarge its applications further.

The Dirac equation plays a fundamental role in various areas of modern physics and mathematics, and is important for the description of interacting particles and fields [40]. Much work about analytically and numerically investigating the nonlinear Dirac (NLD) model has been done; see Ref. [40] and references therein. However, to our knowledge, no research has been done on the LBM for the NLD model in the literature. In this paper, a LB model for the 1D nonlinear Dirac equation (NLDE) is presented by using double complex-valued distribution functions following the idea in Ref. [39]. Unlike the existing LB models with double distribution functions for common coupled convection-diffusion equations and reaction-diffusion system, the equilibrium distribution functions in the present model are selected carefully. Through the Chapman-Enskog expansion, the NLDE can be recovered exactly to the second order of accuracy. Detailed simulations of the NLDE are carried out, and numerical results agree well with the analytical and numerical solutions in the literature.

The rest of the paper is organized as follows. In Sec. II, a LBGK model for NLDE is presented. Numerical tests are

*shibc@hust.edu.cn
†zlguo@hust.edu.cn

made in Sec. III, and finally a brief summary is given in Sec. IV.

II. LBGK MODEL FOR DIRAC EQUATION

The following 1D NLDE is considered in this paper:

$$\partial_t \psi_1 + \partial_x \psi_2 = -i[m - 2\lambda(|\psi_1|^2 - |\psi_2|^2)]\psi_1,$$

$$\partial_t \psi_2 + \partial_x \psi_1 = i[m - 2\lambda(|\psi_1|^2 - |\psi_2|^2)]\psi_2, \tag{1}$$

where ψ_1, ψ_2 are complex-valued functions of time t and position x, $i^2=-1$, and m and λ are real constants.

Motivated by the success of the LB method in modeling both real and complex-valued nonlinear evolution equations [37–39], we establish a LBGK model for solving Eq. (1), a coupled CDE-like equations. The model is based on the one-dimensional, three velocity lattice [2] with double complex-valued distribution functions. The evolution equations of the distribution functions for $\psi_s(s=1,2)$ in the model read

$$f_{sj}(\mathbf{x} + \mathbf{c}_j \Delta t, t + \Delta t) - f_{sj}(\mathbf{x}, t) = -\frac{1}{\tau_s}[f_{sj}(\mathbf{x}, t) - f_{sj}^{\mathrm{eq}}(\mathbf{x}, t)] + \Delta t F_{sj}(\mathbf{x}, t) + \frac{\Delta t^2}{2}\partial_t F_{sj}(\mathbf{x}, t),$$

$$s = 1,2, \quad j = 0,1,2, \tag{2}$$

where $\{\mathbf{c}_0, \mathbf{c}_1, \mathbf{c}_2\} = \{0, c, -c\}$ is the set of discrete velocities, Δx and Δt are the lattice spacing and time step, respectively, $c = \Delta x / \Delta t$ is the particle speed, τ_1, τ_2 are the dimensionless relaxation times, and $f_{1j}^{\mathrm{eq}}(\mathbf{x}, t), f_{2j}^{\mathrm{eq}}(\mathbf{x}, t)$ are the equilibrium distribution functions.

Note that Eq. (1) is a coupled convection equation. In order to recover Eq. (1) from Eq. (2), we chose $f_{sj}^{\mathrm{eq}}(\mathbf{x}, t)$ such that, following our previous work [39],

$$\sum_j f_{sj} = \sum_j f_{sj}^{\mathrm{eq}} = \psi_s, \quad \sum_j \mathbf{c}_j f_{sj}^{\mathrm{eq}} = \psi_{\bar{s}}, \quad \sum_j \mathbf{c}_j \mathbf{c}_j f_{sj}^{\mathrm{eq}} = \psi_s,$$

$$s = 1,2, \tag{3}$$

where $\bar{s} = 3 - s$. Equation (3) leads to

$$f_{s0}^{\mathrm{eq}} = (1 - 1/c^2)\psi_s,$$

$$f_{s1}^{\mathrm{eq}} = \frac{1}{2}(\psi_s/c^2 + \psi_{\bar{s}}/c),$$

$$f_{s2}^{\mathrm{eq}} = \frac{1}{2}(\psi_s/c^2 - \psi_{\bar{s}}/c),$$

$$s = 1,2. \tag{4}$$

F_{sj} in Eq. (2), corresponding to the source terms in Eq. (1), are taken as

$$F_{sj} = \omega_j \left(F_s + \lambda_s \frac{\mathbf{c}_j \cdot F_{\bar{s}}}{c_s^2} \right), \quad s = 1,2, \tag{5}$$

such that

$$\sum_j F_{sj} = F_s, \quad \sum_j \mathbf{c}_j F_{sj} = \lambda_s F_{\bar{s}}, \quad s = 1,2, \tag{6}$$

where $\omega_0 = 2/3$, $\omega_1 = \omega_2 = 1/6$, $c_s^2 = c^2/3$, $F_1 = -i[m - 2\lambda(|\psi_1|^2 - |\psi_2|^2)]\psi_1$, $F_2 = i[m - 2\lambda(|\psi_1|^2 - |\psi_2|^2)]\psi_2$, $\lambda_s = \frac{\tau_s - 1/2}{\tau_s}$, $s = 1,2$ in this paper.

To derive the macroscopic Eq. (1), following the existing LBGK models for CDE, the Chapman-Enskog expansion in time and space is applied,

$$f_{sj} = f_{sj}^{\mathrm{eq}} + \epsilon f_{sj}^{(1)} + \epsilon^2 f_{sj}^{(2)}, \quad F_s = \epsilon F_s^{(1)},$$

$$\partial_t = \epsilon \partial_{t_1} + \epsilon^2 \partial_{t_2}, \quad \partial_x = \epsilon \partial_{x_1}, \quad s = 1,2, \quad j = 0,1,2, \tag{7}$$

where ϵ is a small parameter.

From Eqs. (3), (6), and (7), it follows that

$$\sum_j f_{sj}^{(k)} = 0, \quad (k \geq 1),$$

$$\sum_j F_{sj}^{(1)} = F_s^{(1)}, \quad \sum_j \mathbf{c}_j F_{sj}^{(1)} = \lambda_s F_{\bar{s}}^{(1)},$$

$$s = 1,2, \tag{8}$$

where $F_{sj}^{(1)} = \omega_j (F_s^{(1)} + \lambda_s \frac{\mathbf{c}_j \cdot F_{\bar{s}}^{(1)}}{c_s^2})$, $s = 1,2$. Applying the Taylor expansion and Eq. (7) to Eq. (2), we have

$$O(\epsilon): D_{1j} f_{sj}^{\mathrm{eq}} = -\frac{1}{\tau_s \Delta t} f_{sj}^{(1)} + F_{sj}^{(1)}, \tag{9}$$

$$O(\epsilon^2): \partial_{t_2} f_{sj}^{\mathrm{eq}} + D_{1j} f_{sj}^{(1)} + \frac{\Delta t}{2} D_{1j}^2 f_{sj}^{\mathrm{eq}} = -\frac{1}{\tau_s \Delta t} f_{sj}^{(2)} + \frac{\Delta t}{2} \partial_{t_1} F_{sj}^{(1)}, \tag{10}$$

where $D_{1j} = \partial_{t_1} + \mathbf{c}_j \cdot \partial_{x_1}$. Applying Eq. (9) to the left side of Eq. (10), we can rewrite Eq. (10) as

$$\partial_{t_2} f_{sj}^{\mathrm{eq}} + \left(1 - \frac{1}{2\tau_s}\right) D_{1j} f_{sj}^{(1)} + \frac{\Delta t}{2} D_{1j} F_{sj}^{(1)} = -\frac{1}{\tau_s \Delta t} f_{sj}^{(2)} + \frac{\Delta t}{2} \partial_{t_1} F_{sj}^{(1)}. \tag{11}$$

Deleting $\frac{\Delta t}{2} \partial_{t_1} F_{sj}^{(1)}$ from both sides of Eq. (11), we have

$$\partial_{t_2} f_{sj}^{\mathrm{eq}} + \left(1 - \frac{1}{2\tau_s}\right) D_{1j} f_{sj}^{(1)} + \frac{\Delta t}{2} \mathbf{c}_j \cdot \partial_{x_1} F_{sj}^{(1)} = -\frac{1}{\tau_s \Delta t} f_{sj}^{(2)}. \tag{12}$$

Summing Eqs. (9) and (12) over j, and using Eqs. (3) and (8), we have

$$\partial_{t_1} \psi_s + \partial_{x_1} \psi_{\bar{s}} = F_s^{(1)}, \quad s = 1,2, \tag{13}$$

$$\partial_{t_2} \psi_s + \left(1 - \frac{1}{2\tau_s}\right) \partial_{x_1} \sum_j \mathbf{c}_j f_{sj}^{(1)} + \frac{\Delta t}{2} \partial_{x_1} (\lambda_s F_{\bar{s}}^{(1)}) = 0,$$

$$s = 1,2. \tag{14}$$

Using Eqs. (3), (8), (9), and (13), we have

$$\sum_j \mathbf{c}_j f_{sj}^{(1)} = -\tau_s \Delta t \sum_j \mathbf{c}_j (D_{1j} f_{sj}^{\mathrm{eq}} - F_{sj}^{(1)})$$
$$= -\tau_s \Delta t (\partial_{t_1} \psi_{\bar{s}} + \partial_{x_1} \psi_s - \lambda_s F_{\bar{s}}^{(1)}) = -\tau_s \Delta t (1-\lambda_s) F_{\bar{s}}^{(1)},$$
$$s = 1,2. \tag{15}$$

Then substituting Eq. (15) into Eq. (14), we obtain

$$\partial_{t_2} \psi_s = 0, \quad s = 1,2. \tag{16}$$

Now combining Eqs. (13) and (16), we recover NLDE (1) to the order of $O(\epsilon^2)$. From the analysis above it is found that τ_1 and τ_2 can take any positive values. However, we find that the values of τ_1 and τ_2 around 1 can bring better numerical accuracy and stability of the model (see Sec. III in detail). It is interesting that when $\tau_1 = \tau_2 = 1$, the LB evolution Eq. (2) can be simplified to

$$f_{sj}(\mathbf{x} + \mathbf{c}_j \Delta t, t + \Delta t) = f_{sj}^{\mathrm{eq}}(\mathbf{x}, t) + \Delta t F_{sj}(\mathbf{x}, t) + \frac{\Delta t^2}{2} \partial_t F_{sj}(\mathbf{x}, t),$$
$$s = 1,2, \quad j = 0,1,2, \tag{17}$$

then it follows from Eq. (3) that

$$\psi_s(\mathbf{x}, t + \Delta t) = \sum_j \left[f_{sj}^{\mathrm{eq}}(\mathbf{x} - \mathbf{c}_j \Delta t, t) + \Delta t F_{sj}(\mathbf{x} - \mathbf{c}_j \Delta t, t) + \frac{\Delta t^2}{2} \partial_t F_{sj}(\mathbf{x} - \mathbf{c}_j \Delta t, t) \right], \quad s = 1,2. \tag{18}$$

In this case, the LBGK model becomes a Lax-Wendroff scheme (LWS), also called *finite LB scheme* as in Ref. [41]. However, it should be noted that the analysis in Ref. [41] is on the LB model for fluid and real-valued CDE without the source term, and there is no study of LWS for NDLE in the literature, to our knowledge. Therefore, it is significant to compare the LBGK model with LWS and study the effect of the treatment of source term, which is also one of the main tasks in this paper.

III. SIMULATION RESULTS

To test the LB model proposed above, numerical simulations of NLDE (1) with different boundary conditions are carried out, and we take $\tau_1 = \tau_2 = \tau$ in all simulations. Here we select four test problems as in Ref. [40] for comparison. In simulations, we use the nonequilibrium extrapolation scheme proposed by Guo *et al.* [42] to treat the boundary condition except for the periodic one, and the initial value of each distribution function is taken as that of its equilibrium part at time $t=0$. The explicit difference scheme $\partial_t F_{sj}(\mathbf{x}, t) = [F_{sj}(\mathbf{x}, t) - F_{sj}(\mathbf{x}, t - \Delta t)]/\Delta t$ is used for computing $\partial_t F_{sj}(\mathbf{x}, t)$, $s = 1,2$.

Two LBGK models were used to simulate the first problem which has analytical solutions for comparison. One is the proposed model, and the other is the model using the standard LBGK evolution equation without the term $\frac{\Delta t^2}{2} \partial_t F_{sj}$ in Eq. (2), which are denoted by schemes 1 and 2, respectively. We found that the errors of scheme 2, which is only of first order in time as shown in Ref. [39], are much larger than those of scheme 1 and cannot even be accepted for practical use when lager Δt is used, so the test results of scheme 2 are not listed here. Since the stability of LWS (LBGK scheme with $\tau_1 = \tau_2 = 1$) requires $\Delta t / \Delta x = 1/c \leq 1$, and we found that when $c = 1$ the LBGK model proposed is unstable for evolution with long time, we take $c > 1$ in all simulations here.

The (1+1)-dimensional NLDE (1) has two exact solutions, which will be used in our numerical experiments. The first is the standing-wave solution at $x = x_0$ defined by [40]

$$\boldsymbol{\Psi}^{sw}(x - x_0, t) = [\psi_1^{sw}(x - x_0, t), \psi_2^{sw}(x - x_0, t)]^T = [A(x - x_0), iB(x - x_0)]^T e^{-i\Lambda t}, \tag{19}$$

with

$$A(x) = \frac{a_1 \cosh(bx)}{m + \Lambda \cosh(2bx)}, \quad B(x) = \frac{a_2 \sinh(bx)}{m + \Lambda \cosh(2bx)}, \tag{20}$$

where $a_{1,2} = \sqrt{(m^2 - \Lambda^2)(m \pm \Lambda)/\lambda}$, $b = \sqrt{m^2 - \Lambda^2}$, with $0 < \Lambda \leq m$.

The second exact solution of the Dirac model (1) is the single solitary wave solution placed initially at x_0 with a velocity v [40],

$$\boldsymbol{\Psi}^{ss}(x - x_0, t) = [\psi_1^{ss}(x - x_0, t), \psi_2^{ss}(x - x_0, t)]^T, \tag{21}$$

where

$$\psi_1^{ss}(x - x_0, t) = \sqrt{\frac{\gamma + 1}{2}} \psi_1^{sw}(\tilde{x}, \tilde{t}) + \mathrm{sgn}(v) \sqrt{\frac{\gamma - 1}{2}} \psi_2^{sw}(\tilde{x}, \tilde{t}),$$
$$\psi_2^{ss}(x - x_0, t) = \sqrt{\frac{\gamma + 1}{2}} \psi_2^{sw}(\tilde{x}, \tilde{t}) + \mathrm{sgn}(v) \sqrt{\frac{\gamma - 1}{2}} \psi_1^{sw}(\tilde{x}, \tilde{t}), \tag{22}$$

where $\gamma = 1/\sqrt{1 - v^2}$, $\tilde{x} = \gamma(x - x_0 - vt)$, $\tilde{t} = \gamma[t - v(x - x_0)]$, ψ_1^{sw} and ψ_2^{sw} are defined in Eq. (19), and $\mathrm{sgn}(x)$ is the sgn function, which returns 1 if $x > 0$, 0 if $x = 0$, and -1 if $x < 0$. In simulations, we set $m = 1$, $\lambda = 0.5$ as in Ref. [40].

Example 3.1. (Single traveling solitary wave.) The first example is to simulate traveling of a two-humped Dirac solitary wave. Since the exact single soliton solution (21) to NLDE (1) is known, we can compare our numerical solutions with the exact solution, and then evaluate the accuracy of the proposed model. Here we take $\Lambda = 0.1$, $x_0 = -5$, and $v = 0.1$. The physical domain is considered as $[-25, 25]$, and the initial and boundary conditions are determined by the analytical solution.

Table I gives numerical errors at $t = 100$ and convergence rates for different c and τ. The error is defined by

$$\mathrm{Err} = \frac{\sum_j |\phi(x_j, t) - \phi^*(x_j, t)|}{\sum_j |\phi^*(x_j, t)|}, \tag{23}$$

where ϕ and ϕ^* are the numerical solution and analytical one, respectively, and the summation is taken over all grid points. From the table we can see that our model has the

TABLE I. Example 3.1. Numerical errors and convergence rates of LBGK model for NLDE (1) at $t=100$ [(1) $\tau=0.9$, (2) $\tau=1$, (3) $\tau=1.1$].

Grid N		$c=1.1$				$c=2.0$			
		ψ_1		ψ_2		ψ_1		ψ_2	
		Err	Order	Err	Order	Err	Order	Err	Order
250	(1)	6.64×10^{-2}		8.90×10^{-2}		1.12×10^{-2}		1.28×10^{-2}	
	(2)	1.54×10^{-1}		1.67×10^{-1}		6.87×10^{-2}		6.96×10^{-2}	
	(3)	3.02×10^{-1}		3.04×10^{-1}		1.65×10^{-1}		1.70×10^{-1}	
500	(1)	7.55×10^{-3}	3.1366	9.32×10^{-3}	3.2554	1.87×10^{-3}	2.5824	2.52×10^{-3}	2.3446
	(2)	2.04×10^{-2}	2.9163	2.12×10^{-2}	2.9777	7.24×10^{-3}	3.2462	7.70×10^{-3}	3.1762
	(3)	4.20×10^{-2}	2.8461	4.30×10^{-2}	2.8217	2.09×10^{-2}	2.9809	2.21×10^{-2}	2.9434
1000	(1)	8.36×10^{-4}	3.1749	8.45×10^{-4}	3.4633	8.90×10^{-4}	1.0712	1.07×10^{-3}	1.2358
	(2)	2.88×10^{-3}	2.8244	2.89×10^{-3}	2.8749	7.18×10^{-4}	3.3339	1.03×10^{-3}	2.9022
	(3)	6.20×10^{-3}	2.7600	6.50×10^{-3}	2.7258	2.82×10^{-3}	2.8897	3.29×10^{-3}	2.7479
2000	(1)	1.10×10^{-4}	2.9260	1.13×10^{-4}	2.9026	2.79×10^{-4}	1.6735	3.29×10^{-4}	1.7015
	(2)	4.57×10^{-4}	2.6558	4.79×10^{-4}	2.5930	1.42×10^{-4}	2.3381	2.53×10^{-4}	2.0254
	(3)	1.02×10^{-3}	2.6037	1.10×10^{-3}	2.5629	4.35×10^{-4}	2.6966	5.97×10^{-4}	2.4623
4000	(1)	2.50×10^{-5}	2.1375	4.07×10^{-5}	1.4732	7.70×10^{-5}	1.8573	9.00×10^{-5}	1.8701
	(2)	8.48×10^{-5}	2.4301	9.73×10^{-5}	2.2995	4.75×10^{-5}	1.5799	7.45×10^{-5}	1.7638
	(3)	1.88×10^{-4}	2.4398	2.12×10^{-4}	2.3754	8.12×10^{-5}	2.4215	1.30×10^{-4}	2.1992
8000	(1)	7.05×10^{-6}	1.8262	1.27×10^{-5}	1.6802	2.02×10^{-5}	1.9305	2.35×10^{-5}	1.9373
	(2)	1.80×10^{-5}	2.2361	2.24×10^{-5}	2.1189	1.37×10^{-5}	1.7938	2.03×10^{-5}	1.8758
	(3)	3.90×10^{-5}	2.2692	4.54×10^{-5}	2.2233	1.78×10^{-5}	2.1896	3.09×10^{-5}	2.0728

second-order accuracy in both space and time for fixed c and τ. It should be noted that when the grid number is smaller than or equal to 2000, that is, Δx is larger than or equal to 0.025, the convergent rate is larger than 2.56 for the case of $c=1.1$ and is even larger than 3.46. For this case, the smaller the step, the higher the accuracy.

In order to test further the effect of parameters c and τ on the accuracy and stability of the model, we simulate example 3.1 with different resolutions in detail. The numerical stability regions of relaxation time at $t=100$ for $c=1.1$, $c=1.2$, and $c=2.0$, respectively, are listed in Table II and plotted in Fig. 1, and the *optimal* relaxation times and related minimal er-

TABLE II. Example 3.1. Numerical stability interval $[\tau_{\min},\tau_{\max}]$ and optimal value τ_{opt} of relaxation time, and minimal error and accuracy at $t=100$ [(1) ψ_1, (2) ψ_2].

Grid N		250	500	1000	2000	4000	8000
$c=1.1$		[0.84,1.02],0.86	[0.81,1.40],0.82	[0.82,2.14],0.84	[0.84,3.64],0.87	[0.86,6.67],0.89	[0.87,12.16],0.90
	(1)	4.75×10^{-2}	2.71×10^{-3}	2.65×10^{-4}	6.45×10^{-5}	2.34×10^{-5}	7.05×10^{-6}
			4.1316	3.3542	2.0386	1.4628	1.7308
	(2)	7.14×10^{-2}	4.82×10^{-3}	5.17×10^{-4}	1.07×10^{-4}	4.13×10^{-5}	1.27×10^{-5}
			3.8888	3.2208	2.2726	1.3734	1.7013
$c=1.2$		[0.85,1.04],0.86	[0.83,1.43],0.84	[0.84,2.22],0.87	[0.85,3.81],0.90	[0.87,6.85],0.93	[0.88,6.68],0.94
	(1)	3.12×10^{-2}	1.77×10^{-3}	2.08×10^{-4}	5.52×10^{-5}	1.82×10^{-5}	5.08×10^{-6}
			4.1397	3.0891	1.9138	1.6007	1.8410
	(2)	4.51×10^{-2}	3.21×10^{-3}	3.82×10^{-4}	9.40×10^{-5}	3.07×10^{-5}	9.06×10^{-6}
			3.8125	3.0709	2.0228	1.6144	1.7607
$c=2.0$		[0.86,1.12],0.89	[0.86,1.59],0.92	[0.86,2.57],0.96	[0.88,2.56],0.99	[0.88,2.53],1.01	[0.89,2.51],1.0
	(1)	8.44×10^{-3}	8.88×10^{-4}	3.81×10^{-4}	1.46×10^{-4}	4.60×10^{-5}	1.37×10^{-5}
			3.2486	1.2208	1.3838	1.6663	1.7475
	(2)	1.18×10^{-2}	1.42×10^{-3}	6.80×10^{-4}	2.48×10^{-4}	7.56×10^{-5}	2.03×10^{-5}
			3.0548	1.0623	1.4552	1.7139	1.8969

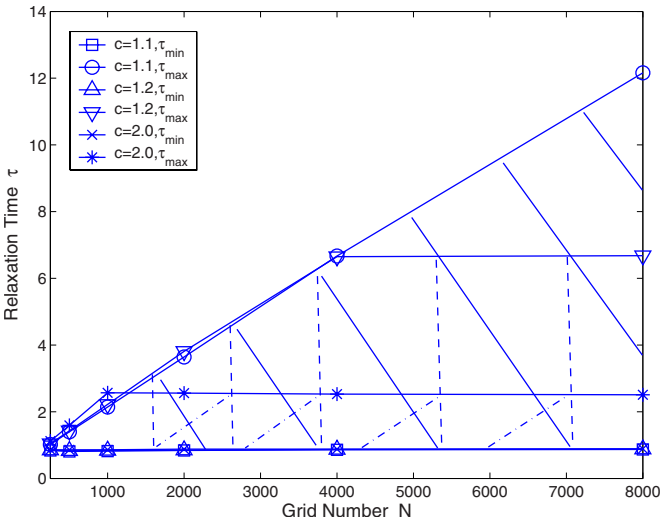

FIG. 1. (Color online) Example 3.1. Stability region of relaxation time τ at $t=100$ for $c=1.1$ (solid line), $c=1.2$ (dashed line), and $c=2.0$ (dashed-dotted line).

rors, as well as accuracy for different Δx and c, are listed in Table II. Here, the criterion of stability is chosen as Err <0.2. The analytic solutions vs numerical solutions at $t=0$ and $t=100$ for $\Delta x=0.01$ and $\Delta t=0.001$ are plotted in Fig. 2, which shows that the numerical solution is in excellent agreement with analytic one.

From Table II and Fig. 1, it can be found that the stability region for $c=1.1$ is much larger than that for $c=2.0$, and it becomes larger for fixed Δx as c decreases. We also found that better accuracy is obtained in a small region with $\tau \leqslant 1.1$ for all the cases tested, and the relaxation time τ responding to the minimal error for each resolution is less than 1 when c is near 1 or Δt is large, otherwise the best τ is much closer or equal to 1 when c is larger. For fixed Δx, the proposed model may be more accurate if we select c and τ properly.

The long-time evolution of the global relative errors for $\Delta x=0.01$ and different τ and c is shown in Fig. 3. It can be

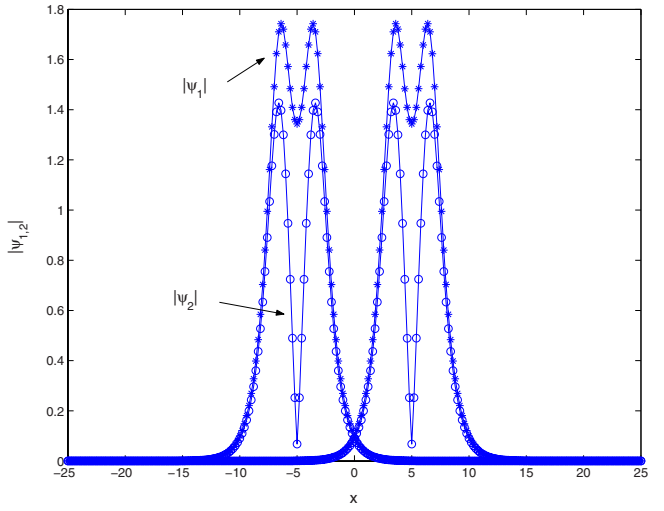

FIG. 2. (Color online) Example 3.1. Analytic solutions (solid) vs numerical solutions (symbol) at $t=0$ (left) and $t=100$ (right) for $\tau=1$, $\Delta x=0.01$ and $c=10$.

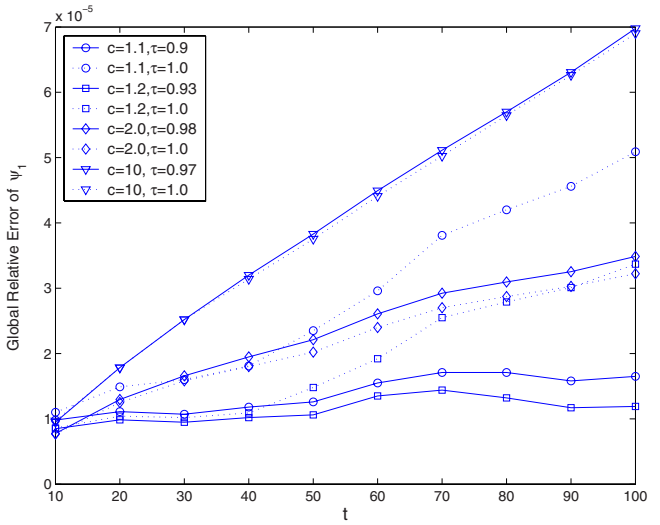

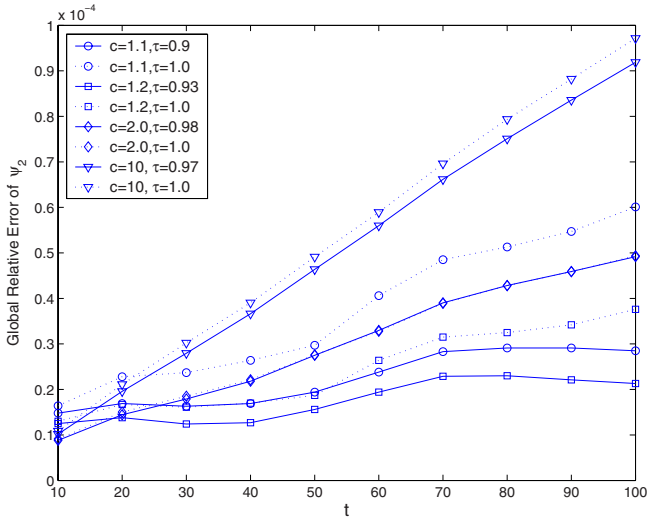

FIG. 3. (Color online) Example 3.1. The time evolution of the global relative errors for $\Delta x=0.01$, and different τ and c. Top: ψ_1; bottom: ψ_2.

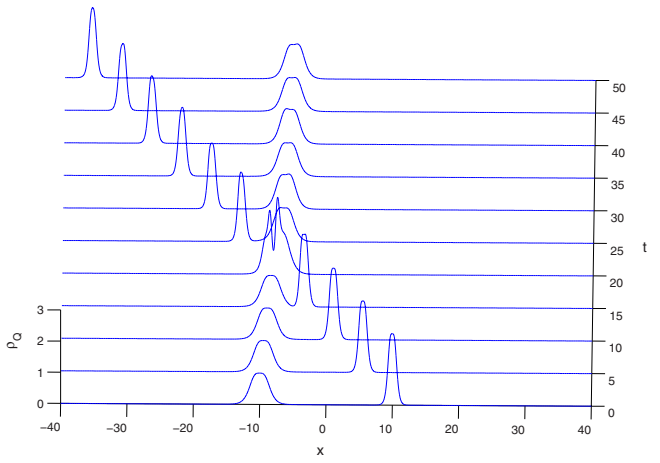

FIG. 4. (Color online) Example 3.2. The time evolution of the charge density ρ_Q obtained by the present model. $\tau=1$, $\Delta x=0.01$, $\Delta t=0.001$.

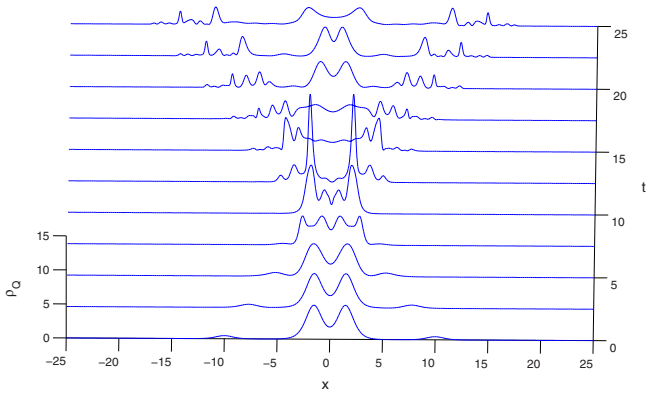

FIG. 5. (Color online) Example 3.3. The time evolution of the charge density ρ_Q obtained the present model. $\tau=1$, $\Delta x=0.01$, $\Delta t=0.001$.

found that the oscillation of errors for $\tau<1$ is less than those for $\tau=1$, when c is near 1 or Δt is large, while for larger c the error increases faster as t increases, and the better accuracy is attained as τ approaches 1.

The numerical results above show that the LBGK model is comparable to the method in Ref. [40], and with a large Δt the LBGK scheme is better than the Lax-Wendroff one if τ is suitably selected.

Example 3.2. (Binary collisions.) This example involves collisions of two one-humped solitary waves with a phase shift of π, i.e., Eq. (1) is subject to the initial data

$$\mathbf{\Psi}(x,0) = \mathbf{\Psi}^{ss}(x-x_l,0) + \mathbf{\Psi}^{ss}(x-x_r,0), \tag{24}$$

with $\Lambda_l=\Lambda_r=0.5$, $v_l=0.1$, $v_r=-0.9$, and $x_l=-x_r=10$. Here we take the physical domain $[-40,40]$. The time evolution of the charge density $\rho_Q(x,t)=|\psi_1|^2+|\psi_2|^2$ obtained by the present model is plotted in Fig. 4.

Example 3.3. (Ternary collisions.) The third example is to consider collisions of three in-phase Dirac solitary waves. The initial data are specified as follows:

$$\mathbf{\Psi}(x,0) = \mathbf{\Psi}^{ss}(x-x_l,0) + \mathbf{\Psi}^{ss}(x-x_m,0) + \mathbf{\Psi}^{ss}(x-x_r,0), \tag{25}$$

with $\Lambda_l=\Lambda_r=0.9$, $\Lambda_m=0.1$, $v_l=-v_r=0.9$, and $v_m=0$. Here we take the physical domain $[-25,25]$. The time evolution of the charge density ρ_Q obtained by the present model is plotted in Fig. 5.

Example 3.4. (Quadruple collisions.) The final example is to study quadruple collisions of the Dirac waves. The initial data are given as

$$\mathbf{\Psi}(x,0) = -\mathbf{\Psi}^{ss}(x-x_l,0) + \mathbf{\Psi}^{ss}(x-x_{lm},0) + \mathbf{\Psi}^{ss}(x-x_{rm},0) - \mathbf{\Psi}^{ss}(x-x_r,0), \tag{26}$$

with $\Lambda_l=\Lambda_r=\Lambda_{lm}=\Lambda_{rm}=0.5$, $v_l=v_r=v_{lm}=v_{rm}=0$, $x_l=-x_r=15$, and $x_{lm}=-x_{rm}=5$. Here we take the physical domain $[-50,50]$. The time evolution of the charge density ρ_Q obtained by scheme 1 is plotted in Fig. 6. From Figs. 4–6 it is found that the numerical results obtained by the present model agree excellently with those in Ref. [40].

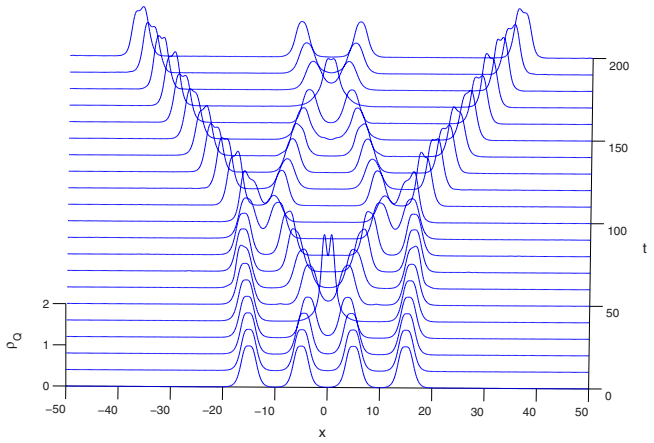

FIG. 6. (Color online) Example 3.4. The time evolution of the charge density ρ_Q obtained the present model. $\tau=1$, $\Delta x=0.01$, $\Delta t=0.001$.

IV. CONCLUSION

In the present work, we have developed a LBGK model for 1D NLDE by using double complex-valued distribution functions. Unlike traditional numerical methods which solve the equations for macroscopic variables, the present model has the advantages of standard LBGK method, such as simplicity and symmetry of scheme, ease in coding, and intrinsical parallelism [3]. The effects of space and time resolutions and relaxation time on the accuracy and stability of the model are investigated through detailed simulations of four test problems. It is found that the model is higher than the second-order accuracy in both space and time, and its convergent rate is near 3.0 at lower grid resolutions, even larger than 4.0 for properly selected relaxation time, which shows that the LBM has potentials in simulating NLDE. The existing LB models may be directly applied to NLDE (1) by using the idea of the proposed model. It is worth noticing that reasonable physical explanation and deep analysis of the model are still needed in future, which is helpful to the development and application of LB model.

ACKNOWLEDGMENTS

The authors are grateful to referees for their valuable comments and suggestions. This work is supported by the National Science Foundation of China (Grants No. 60773195 and No. 50606012).

[1] R. Benzi, S. Succi, and M. Vergassola, Phys. Rep. **222**, 145 (1992).
[2] Y. H. Qian, S. Succi, and S. A. Orszag, Annu. Rev. Comput. Phys. **3**, 195 (1995).
[3] S. Chen and G. D. Doolen, Annu. Rev. Fluid Mech. **30**, 329 (1998).
[4] F. J. Higuera, S. Succi, and R. Benzi, Europhys. Lett. **9**, 345 (1989).
[5] D. d'Humières, in *Rarefied Gas Dynamics: Theory and Simulations*, Progress in Astronautics and Aeronautics Vol. 159, edited by B. D. Shizgal and D. P. Weaver (AIAA, Washington, DC, 1992), pp. 450–458.
[6] P. Lallemand and L.-S. Luo, Phys. Rev. E **61**, 6546 (2000).
[7] I. V. Karlin, A. Ferrante, and H. C. Ottinger, Europhys. Lett. **47**, 182 (1999).
[8] S. Ansumali, I. V. Karlin, and H. C. Ottinger, Europhys. Lett. **63**, 798 (2003).
[9] S. S. Chikatamarla, S. Ansumali, and I. V. Karlin, Phys. Rev. Lett. **97**, 010201 (2006).
[10] B. M. Boghosian, J. Yepez, P. V. Coveney, and A. Wagner, Proc. R. Soc. London, Ser. A **457**, 717 (2001).
[11] B. Keating, G. Vahala, J. Yepez, M. Soe, and L. Vahala, Phys. Rev. E **75**, 036712 (2007).
[12] S. P. Dawson, S. Y. Chen, and G. D. Doolen, J. Chem. Phys. **98**, 1514 (1993).
[13] R. Blaak and P. M. Sloot, Comput. Phys. Commun. **129**, 256 (2000).
[14] X. M. Yu and B. C. Shi, Appl. Math. Comput. **181**, 958 (2006).
[15] M. R. Swift, E. Orlandini, W. R. Osborn, and J. M. Yeomans, Phys. Rev. E **54**, 5041 (1996).
[16] Z. L. Guo, B. C. Shi, and N. C. Wang, J. Sci. Comput. **14**, 291 (1999).
[17] X. Y. He, N. Li, and B. Goldstein, Mol. Simul. **25**, 145 (2000).
[18] R. G. M. van der Sman and M. H. Ernst, J. Comput. Phys. **160**, 766 (2000).
[19] R. G. M. van der Sman, Phys. Rev. E **74**, 026705 (2006).
[20] B. C. Shi, B. Deng, R. Du, and X. W. Chen, Comput. Math. Appl. **55**, 1568 (2008).
[21] X.-M. Yu and B.-C. Shi, Chin. Phys. **15**, 1441 (2006).
[22] Z. H. Chai, B. C. Shi, and L. Zheng, Chaos, Solitons Fractals **36**, 874 (2008).
[23] Z. H. Chai and B. C. Shi, Appl. Math. Model. **32**, 2050 (2008).
[24] X. X. Zhang *et al.*, Adv. Water Resour. **25**, 1 (2002).
[25] I. Rasin, S. Succi, and W. Miller, J. Comput. Phys. **206**, 453 (2005).
[26] I. Ginzburg, Adv. Water Resour. **28**, 1171 (2005).
[27] D. A. Meyer, J. Stat. Phys. **85**, 551 (1996).
[28] S. Succi and R. Benzi, Physica D **69**, 327 (1993).
[29] S. Succi, Phys. Rev. E **53**, 1969 (1996).
[30] B. Boghosian and W. Taylor IV, Int. J. Mod. Phys. C **8**, 705 (1997).
[31] J. Yepez and B. Boghosian, Comput. Phys. Commun. **146**, 280 (2002).
[32] J. Yepez, J. Stat. Phys. **107**, 203 (2002).
[33] G. Vahala, J. Yepez, and L. Vahala, Phys. Lett. A **310**, 187 (2003).
[34] G. Vahala, L. Vahala, and J. Yepez, Physica A **362**, 215 (2006).
[35] S. Palpacelli and S. Succi, Phys. Rev. E **75**, 066704 (2007); **77**, 066708 (2008).
[36] S. Palpacelli and S. Succi, Commun. Comput. Phys. **4**, 980 (2008).
[37] L. H. Zhong, S. D. Feng, P. Dong, and S. T. Gao, Phys. Rev. E **74**, 036704 (2006).
[38] B. C. Shi, Lect. Notes Comput. Sci. **4487**, 818 (2007).
[39] B. C. Shi and Z. L. Guo, Phys. Rev. E **79**, 016701 (2009).
[40] H. Wang and H. Z. Tang, J. Comput. Phys. **222**, 176 (2007).
[41] R. G. M. van der Sman, Comput. Fluids **35**, 849 (2006).
[42] Z.-L. Guo, C.-G. Zheng, and B.-C. Shi, Chin. Phys. **11**, 366 (2002).